Program Digest, 2019 IEEE International Ultrasonics Symposium (IUS)
Glasgow, Scotland, October 6-9, 2019

Real-Time Thermoacoustic Imaging and Thermometry during Focused Microwave Heating in Multilayer Breast Phantom

Chandra Karunakaran
Dept. of Medical Imaging
University of Arizona
Tucson, AZ, USA
chandrapriya13@gmail.com

Srishti Saraswat
Dept. of Electrical and Computer Eng.
University of Arizona
Tucson, AZ, USA
srishtis@email.arizona.edu

Jinpil Tak
Dept. of Electrical and Computer Eng.
University of Arizona
Tucson, AZ, USA
abrahamtak@email.arizona.edu

Hongbo Zhao
Dept. of Electrical and Computer Eng.
University of Arizona
Tucson, AZ, USA
zhaohb@email.arizona.edu

Hao Xin
Dept. of Electrical and Computer Eng.
University of Arizona
Tucson, AZ, USA
hxin@email.arizona.edu

Russell S Witte
Dept. of Medical Imaging
University of Arizona
Tucson, AZ, USA
rwitte@email.arizona.edu

***Abstract*—This study describes real-time thermoacoustic imaging (TAI) and thermometry (TAT) for feedback during thermal therapies. The system uses a linear ultrasound array and imaging system to noninvasively estimate temperature. The system was validated in gel phantoms, muscle and fat tissue samples. A mean error between 10 and 20% per degree was observed for estimating temperature. A TAT system using a single element ultrasound probe was also integrated with a focused microwave therapy (FMT) setup for generating local heating, leading to a mean error of 1.18±0.87 °C compared to thermocouples placed near the region of interest. The results support the long-term goal of developing a closed-loop platform for image-guided ablation therapy for breast cancer.**

Keywords*—*radiofrequency ablation, hyperthermia, focused microwave therapy, breast cancer

I. INTRODUCTION

In recent years, there has been a progressive trend towards minimally invasive treatments for breast cancer, such as ablation using extreme heat (e.g., with radiofrequencies (RF), focused ultrasound) or cold (cryoablation). These thermal ablation techniques have advantages compared to breast conservation surgery, such as better cosmetic preservation and less systemic side effects [1]. However, control of the thermal dose is difficult using these therapies. Whereas thermocouples are invasive and provide only point measurements, MR thermometry requires expensive equipment. Ultrasound imaging and thermometry is a low-cost option but lacks sensitivity and accuracy. Microwave imaging has inherent contrast but has limited spatial resolution (>1 cm). As a result, there remains an unmet need for an accurate, real-time, low cost modality for monitoring temperature during ablation therapy.

Thermoacoustic imaging (TAI) involves an incident microwave pulse, transient heating in tissue, thermoelastic expansion, and production of broadband pressure signals, which are then detected by ultrasound receivers to form a high contrast and high-resolution image. TAI has been studied extensively and found applicable in tumor imaging [2] and non-invasive thermometry [3]. The linear correlation between temperature and TAI signal is related to the Grüneisen parameter, which describes efficiency of thermal energy conversion to pressure and depends on the tissue composition.

Most of the above-mentioned studies used either a single element ultrasound transducer to slowly scan the treatment area or required custom ultrasound transducers and electronics, which was expensive and more difficult to reproduce [3]. Another study [4] used a commercial 2.5 MHz linear array (Phillips P4-1) and an ultrasound platform for TAI imaging of prostate cancer but did not implement TAI based thermometry. Our study outlines the use of a commercially available linear ultrasound array for real-time 2D TAI and thermometry.

The ultimate goal of the study is to integrate TAI thermometry with focused microwave therapy (FMT) for treatment of breast cancer. In FMT, microwave energy can be noninvasively focused to cause hyperthermia or ablation with the added advantage of good depth penetration and resolution due to differential microwave absorption inherent in different tissue types [5]. FMT can benefit from real-time, TA imaging and thermometry to serve as feedback for therapy monitoring and guidance. In this study, we report the performance of TAI/TAT in gel phantoms, muscle and fat tissue during slow convection heating. We also demonstrate integration of real-time TAT with a custom four-element focused microwave platform for combining local heating with imaging and thermometry.

II. METHODS

A. TAI with a linear ultrasound array

A microwave source (EPSCO Model PG5KB) was used to produce short microwave pulses (2.8 GHz, 4 KW peak, 340 ns) for TA imaging. The microwave energy is directed into the imaging tank through a waveguide and matching layer.

As illustrated in Figure 1, TA signals were acquired with a 96-element 2.5 MHz linear ultrasound array (P4-1, Philips) on a commercial ultrasound platform (Vantage 64LE, Verasonics).

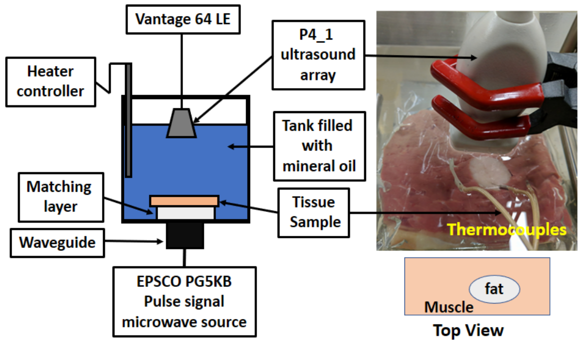

Fig. 1. Setup for TAI and thermometry in *ex-vivo* muscle and fat samples.

B. Multilayer breast phantom

A multilayer breast tissue mimicking phantom was fabricated by adding gelatin to emulsions with different oil-water ratios to match tissue dielectric properties found in breast tissue, including skin, glandular, transitional and fat [6]. The peak TA signals from the various tissue layers were characterized and shown in Figure 2 and consistent with their conductivity.

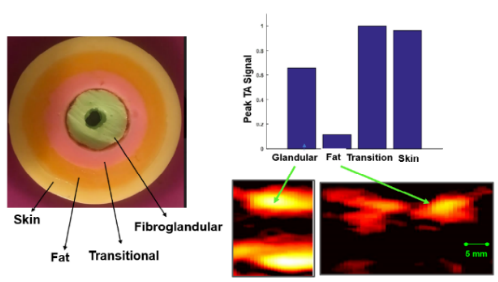

Fig. 2: Multilayer breast phantom. Color coding indicates Skin, Fat, Transitional and Fibroglandular samples. Comparison of peak TA signal from different tissue gel phantom ***types.***

C. Tissue preparation and temperature estimation

A slab of fresh bovine muscle with embedded porcine fat (0.5 cm thick) was wrapped in a thin film, before placing in the imaging tank filled with mineral oil, maintained at 60°C through a heating element and a controller. Needle thermocouples were placed in the fat and muscle samples to record temperature every second during heating.

The setup and sample are displayed in Figure 1. Average TA images were recorded every 5 seconds or sooner. The peak TA signal in defined regions within the muscle and fat tissue were then correlated with the thermocouple measurements, and the best-fit lines were calculated. A second validation experiment was repeated with the same sample by letting the sample cool between experiments. Change in sample temperatures were estimated based on eqn. (1), with slope values calculated from the calibration experiment. Temperature change (ΔT) at time t_n can be estimated from,

$$\Delta T(t_n) = \frac{TAI(t_n) - TAI(t_0)}{Slope} \quad (1)$$

Where, $TAI(t_n)$ and $TAI(t_0)$ are peak TAI signals calculated at the region of interest (ROI) for time t_n and t_0, respectively. *Slope* refers to the slope calculated between the TAI signal and temperature from the calibration experiments. Measured temperatures were compared with estimated temperatures for fat and muscle samples to assess accuracy of TA thermometry.

D. Integrated TAI-FMT

Following the validation of TAI in imaging and thermometry with *ex-vivo* tissue samples with passive heating, we tested a modified system for estimating temperature *during* focused microwave heating. The setup for integrated TAI-FMT is displayed in Figure 3, which consists of a 3D printed FMT chamber placed on top of a dielectric matching layer to help direct microwave energy into the FMT chamber. Four custom designed microwave patch antennae (915 MHz) were attached to the walls of the FMT chamber, such that the four antennae formed a focus at the center of the sample. The FMT setup is explained in detail in [8]. For focused microwave therapy, continuous energy is generated by an RF source (E8257C, PSG Analog Signal Generator, Agilent Technologies) amplified by power amplifiers (10 W) before outputting to the antennae. The sample consisted of a 0.9% saline-agarose gel placed inside the FMT chamber filled with deionized water. The saline gel, with higher microwave absorption, acts as target for the focused microwave energy.

Five type-T wire thermocouples were inserted in the sample and temperatures were recorded throughout the experiment using a datalogger (TC-08, Pico Technology). For TA imaging, continuous microwave energy was generated through a source (Agilent N5182A MXG Vector Signal Generator) and amplified (177L Band Amplifier, Applied Systems Engineering) before limiting the output pulse width (1 µs, 500 PRF, 5 KW peak) through an external trigger.

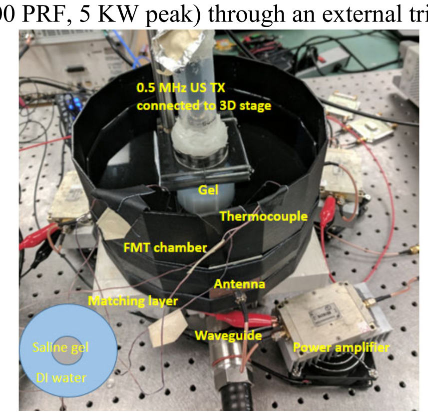

Fig 3: Integrated TAI-FMT setup.

The amplifier output was triggered to control the microwave pulse-width and energy, which was directed into the FMT chamber from the bottom through the matching layer.

A 0.5 MHz (Olympus Panametrics NDT V389) focused, single element transducer was attached to a 3D motorized stage and scanned along the sample to record thermoacoustic image cross-sections periodically during the heating experiment. A lower frequency was chosen to acquire TA images with better signal-to-noise ratio (SNR) compared to 2.5 MHz. Thermoacoustic signals were filtered through a pulser-receiver (Olympus 5072PR), amplified (59 dB) and recorded using a NI DAQ (NI PXI-5922) acquisition system. 2D pulse-echo images were obtained before and after the microwave heating by scanning the ultrasound transducer to obtain B mode ultrasound images. The imaging setup is explained in detail in a previous study [7]. TAI images were obtained every five minutes throughout the 85-minute focused microwave heating by scanning the ultrasound transducer over the area with the 3D positioner. Although TA scans could be performed more frequently (every 30 seconds), five minutes between scans allowed for significant heating from the focused microwave setup. 2D pixel-wise slope calculations were performed which were then used to estimate 2D temperature maps based on calculated average slope. Sound speed changes induced by temperature can cause a shift in the position of the peak TA signal within subsequent frames and hence need to be accounted for while calculating 2D slope maps.

III. Results

Results from a representative tissue thermometry experiment using the 2.5 MHz linear array are depicted in Fig. 4. Pulse-echo image (4a) shows hyperechoic fat to the right of the image and muscle to the left. The corresponding TA image is shown in panel b, where bright signals are seen from the top and bottom of the muscle sample, whereas much weaker signals are observed from the bottom of the fat sample due to the inherent differences in microwave absorption between muscle and fat. In correlating peak TAI signals from the muscle and fat ROIs (shown in 3b), slopes of 1.6 % per °C (R^2=0.65) and 2.4% per °C (R^2=0.88) were obtained for muscle and fat respectively (4c & 4d).

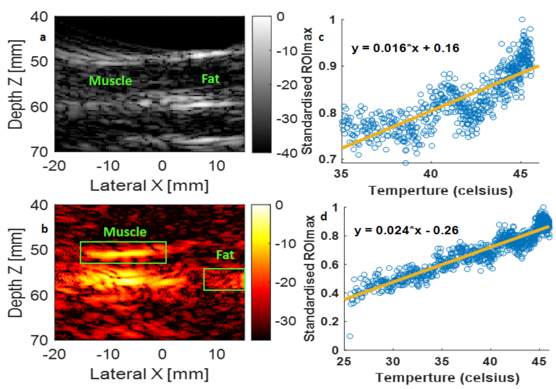

Fig 4: Pulse-echo (a) image and corresponding thermoacoustic image (b) depicting muscle and fat regions in the sample. Green boxes identify the ROIs used for TA signal calculation Peak TAI signal in ROI versus temperature correlation for muscle (c) and fat (d).

The slopes calculated from the calibration experiments were then used to estimate temperatures in a second set of validation experiments, and the results are displayed in Fig. 5. The sample was allowed to cool and then reheated using the same protocol as previously described. The instantaneous change in TA signal was used to estimate temperature changes based on (1). Comparison of measured and estimated temperature profiles for muscle and fat are revealed in Fig. 5a and 5b, respectively. Experiments were repeated with different samples and the same validation protocol was followed. The summary of estimated slopes and temperatures for fat and muscle across experiments are presented in Fig. 5c and 5d. Averaged slopes for fat, muscle and saline were 2.23%, 1.53% and 2% per °C, respectively. Average RMS errors across experiments in estimating temperature were 19.1% and 13.9% per °C respectively for fat and muscle. In estimating temperature, a higher error (19.1%) was observed for fat compared to muscle, which is likely due to lower SNR from fat.

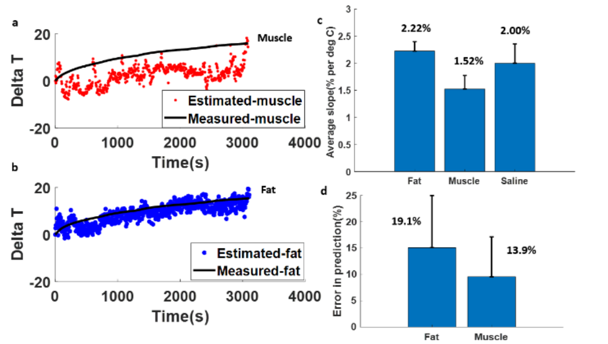

Fig 5: Temperature estimation in muscle (a) and fat (b). Summary of slopes (c) and error in temperature estimation (d) for muscle and fat.

Results from a representative TAI-FMT experiment are displayed in Fig. 6 and 7. The pulse echo and corresponding TA images in Fig. 6 clearly reveals the top and bottom boundary of the saline gel. The location of the thermocouples (denoted by T1 through T5) are indicated in the pulse echo image, whereas the corresponding ROIs (denoted by R1 through R5) are illustrated in the TA image. Temperature profiles across the gel during heating as measured by the five thermocouples indicate differential heating with maximum temperature increases at the center locations (T1 and T4). The TA signal vs. temperature slope at the center thermocouple location T1 is shown in Figure 6d with an average value of 2.3% (R^2= 0.939). Such slope calculations were performed at all five thermocouple locations and corresponding ROIs. The calculated slopes at the other four thermocouple locations were 2.8% (R^2=0.95), 2.14% (R^2=0.95), 2.12% (R^2=0.92) and 2.18% (R^2=0.59) at T5, T4, T2 and T3 respectively. The slopes at the five thermocouple locations were averaged, since the gel is uniform, to obtain an average slope of 2.3±0.28% per °C which was then used in estimating temperature for the entire image.

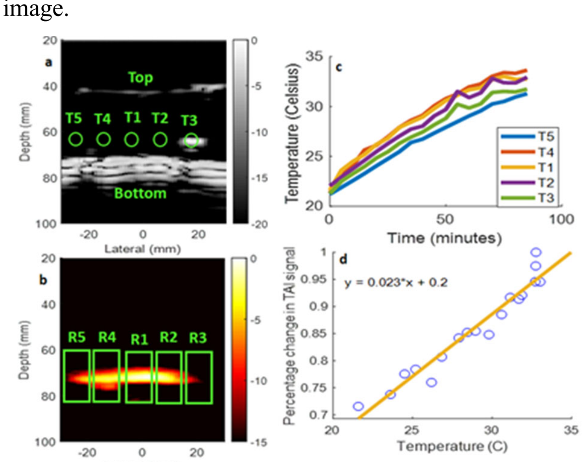

Fig 6: Pulse-echo (a) and thermoacoustic (b) images of saline gel sample in TAI-FMT experiment. Thermocouple locations are identified by circles T1 through T5, corresponding ROIs are identified by rectangles R1 through R5. FMT heating profile across the gel at locations T1 through T5 (c) and TA signal-temperature correlation at location T3 (d).

Comparison of measured and estimated temperatures at the five thermocouple locations, T1 through T5, is shown in Fig 7a. RMS errors between measured and estimated temperatures for the five locations individually and altogether is shown in

Table 1 The overall error was 1.18 °C with RMS errors at the individual locations being 1.12 °C (T5), 1.92 °C (T4), 0.99 °C (T1), 1.16 °C (T2) and 3.58 °C (T5). Following point-wise temperature estimation, the change in TA signal were calculated over the whole TA image and 2D temperature estimation maps for various time points in the experiments were obtained using the average slope of 2.3% per Celsius. The 2D maps have been corrected for TA signal shift due to change in sound speed with heating by calculating the shift using cross-correlation and correcting for the shift. Representative 2D TA thermometry maps at 20 mins, 40 mins and 85 mins during FMT are shown in Figures 6b-6d. The TAI technique was able to estimate real-time temperature changes pixel-by-pixel with a total temperature rise of 15-20 °C at the end of the focused microwave exposure.

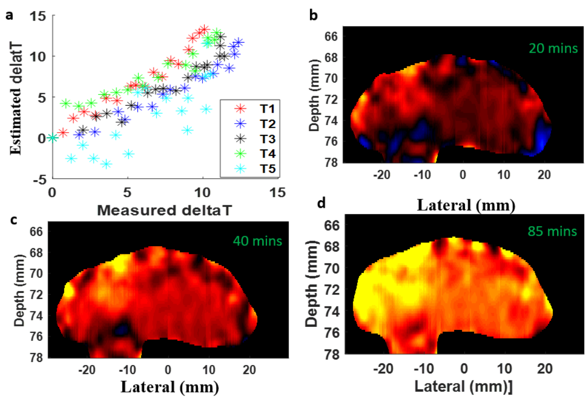

Fig 7: Pixel-wise comparison of measured and estimated temperatures at thermocouple locations T1 through T5 (a) and 2D temperature estimation maps at 20 mins (b), 40 mins (40) and 85 mins (d) during FMT. TA signal shift due to sound speed changes have been corrected by cross correlation.

Location	Measured ΔT (°C)	Error (°C)	Error (%)
T1	11.17	1.12±1.05°C	11.13%
T2	10.91	1.92±0.84°C	15.55%
T3	10.49	0.99±0.9°C	8.74%
T4	12.36	1.16±1.02°C	10.7%
T5	10.09	3.58±2.71°C	34.2%
Overall		1.18±0.87°C	9.58%

Table 1: Temperature estimation error across five thermocouple locations

IV. Discussion

While the TAI/TAT system was able to accurately estimate temperatures, a mismatch between the location of the thermocouple and regions of interest likely contributed to some inaccuracies in the slope and temperature estimations, as is evident in the RMS errors at the five thermocouple locations. RMS error was the least at location T1 (0.99 °C), where the expected slope was consistent with the actual slope (2.3%). A higher error of 3.58 °C occurred near T3. Although thermocouple locations are confirmed in the pulse-echo images, there still exists mismatch between the actual thermocouple location and the location from where TA signals are calculated, which could attribute to errors in slope calculation, especially in non-uniform samples. Also, lower SNR may lead to lower correlations as observed at location T3 (R^2=0.59). While we currently have only five-point temperature measurements, our future work will include a 2D measured temperature map, either through physical measurements or through modeling.

In correcting for temperature-induced sound speed changes, currently, a 1D cross-correlation between frames was performed and used in correcting for the axial shift. In the future, we aim to include sound speed changes between frames in the 2D temperature estimation. For future studies, the imaging will be performed with custom designed 3D arrays optimized for the microwave pulse parameters.

While we have assumed gel uniformity and calculated the averaged slope for estimating temperature, this will likely not be accurate for heterogeneous tissue, such as adipose and granular breast tissues. For future experiments, our goal is to develop 2D and 3D slope maps, where slopes will be calculated at each pixel in the 2D image. The location-specific slopes will then be used to estimate temperatures superimposed on 2D and 3D TA images.

In summary, we have implemented real-time TA imaging and thermometry on a commercial ultrasound platform and clinical linear ultrasound array. Additionally, we have validated the technique for thermometry in different types of tissue and integrated it with an early-prototype focused microwave heating system. The overall goal of this study is to develop a noninvasive TAI/TAT/FMT platform for image-guided thermal therapy and improving outcomes for patients with breast cancer.

V. References

[1] Z Zhao and F Wu, “Minimally Invasive Thermal Ablation of Early-stage Breast Cancer: A Systemic review,” in EJSO 36 (2010): 1149-155.

[2] RA Kruger, KD Miller, HE Reynolds, WL Kiser, Dr Reinecke, GA Kruger, “Breast Cancer in vivo: Contrast Enhancement with thermoacoustic CT at 434 MHz-Feasibility Study”. Radiology 2000 (216) ,1: 279-283.

[3] C Lou, D Xing, “Temperature Monitoring Utilizing Thermoacoustic Signals During Pulsed Microwave Thermotherapy: A Feasibility Study,” Int. J. Hyperthermia 2010, 26(4): 338-346.[4]

[4] SK Patch, WA See, “VHF-induced Thermoacoustic Imaging of Fresh Human Prostrates Using a Clinical Ultrasound Transducer Array,” Proc. of SPIE vol. 9708.

[5] J Stang, M Haynes, P Carson, M Moghaddam, “A Preclinical System Prototype For Focused Microwave Thermal Therapy of the Breast”, IEEE Trans. Biomed. Eng. 2012; 59(9): 2431-2438.

[6] Stang JP, Ward C, van Nieuwstadt L, Fabiilli M, Haynes M, Carson P, Moghaddam M. Customizable emulsion matching media and tissue mimicking phantoms for microwave breast imaging and therapy. Phys Med Biol. in preparation (draft available).

[7] D Bauer, X Wang, J Violin, H Xin, RS Witte. Spectroscopic Thermoacoustic Imaging of Water and Fat Composition. Appl. Phys. Lett., 101 (2012).

[8] S Saraswat, J Tak, M Liang, C Lyu, RS Witte, H Xin. Towards Study on Thermoacoustic Imaging Guided Focused Microwave Therapy for Breast Cancer Treatment. *IEEE/MTT-S International Microwave Symposium – IMS* 2018, 953-956.

This work is supported by DOD CDMRP Grant # W81XWH-16-1-0423
We acknowledge the UA Center for Gamma Ray Imaging (CGRI) for the use of their 3D printer.